LETTERS
PUBLISHED ONLINE: 14 SEPTEMBER 2014 | DOI: 10.1038/NGEO2247
nature geoscience

Global assessment of trends in wetting and drying over land

Peter Greve[1,2]*, Boris Orlowsky[1], Brigitte Mueller[1†], Justin Sheffield[3], Markus Reichstein[4] and Sonia I. Seneviratne[1]*

Changes in the hydrological conditions of the land surface have substantial impacts on society[1,2]. Yet assessments of observed continental dryness trends yield contradicting results[3–7]. The concept that dry regions dry out further, whereas wet regions become wetter as the climate warms has been proposed as a simplified summary of expected[8–10] as well as observed[10–14] changes over land, although this concept is mostly based on oceanic data[8,10]. Here we present an analysis of more than 300 combinations of various hydrological data sets of historical land dryness changes covering the period from 1948 to 2005. Each combination of data sets is benchmarked against an empirical relationship between evaporation, precipitation and aridity. Those combinations that perform well are used for trend analysis. We find that over about three-quarters of the global land area, robust dryness changes cannot be detected. Only 10.8% of the global land area shows a robust 'dry gets drier, wet gets wetter' pattern, compared to 9.5% of global land area with the opposite pattern, that is, dry gets wetter, and wet gets drier. We conclude that aridity changes over land, where the potential for direct socio-economic consequences is highest, have not followed a simple intensification of existing patterns.

The 'dry gets drier, wet gets wetter' (DDWW) paradigm has become a standard catchphrase frequently used in studies and assessments of historical and future climate change[8,9,11–13]. However, remaining large uncertainties in assessments of past changes[3–7,13] and the fact that historical assessments of the DDWW paradigm are based on oceanic evidence[8,10,15,16], require a careful re-evaluation of its validity over land. The choice of data constitutes an essential source of uncertainty, owing to the large number and diversity of existing hydrological data sets[6,17,18]. Here we circumvent these issues through the analysis of an unprecedentedly large selection of evapotranspiration (E), precipitation (P) and potential evaporation (E_p) data sets and their combinations. Another issue lies in the use of different measures for changes in dryness or wetness, which often only take single components of the water balance into account[3,4,6,19]. In addition, also the definition of 'dry' versus 'wet' regions can be problematic. For instance, they cannot be characterized with negative versus positive $P–E$ values over land (unlike for ocean areas[8]) because $P–E$ is overwhelmingly positive on continents (Supplementary Information). We address these issues here by applying an improved metric that is more relevant for climate impacts to global land regions for the historical period 1948–2005. Thereby, we directly investigate dryness changes in the phase space spanned by the water balance at the land surface ($P–E$) and by considering potential hydroclimatological regime shifts in the aridity index E_p/P. 'Dry' versus 'wet' climate regimes are based on well-established definitions from the hydrological literature[20].

In a first step, the combinations of E, P and E_p data sets are evaluated for physical consistency using the Budyko framework[21]. To maximize the number of available data sets and, in particular, to include a sufficient number of observation-based data sets, we choose the 1984–2005 time frame for validation. Over this period, we evaluate all combinations against the Budyko framework[16,21–26], which provides a well-established and both empirically and theoretically solid functional relationship relating the evaporative index E/P to the aridity index E_p/P. This approach permits a direct evaluation of the individual combinations of E, P and E_p data sets, without evaluating single data sets first. The aridity index captures the competing effects of land water supply and atmospheric water demand, with the former (latter) being dominant for $E_p/P > 1$ ($E_p/P < 1$). We use the following formulation of Budyko's relationship[22],

$$\frac{E}{P} = 1 + \left(\frac{E_p}{P}\right) - \left(1 + \left(\frac{E_p}{P}\right)^{\omega}\right)^{\frac{1}{\omega}} \quad (1)$$

which includes the free parameter ω, being related to the climatological normalized density vegetation index[26] (NDVI) and therefore accounting for vegetation influences[24] (Methods). Both ratios are computed from climatological annual averages of the 1984–2005 period. Note that this adjusted Budyko curve is still a rough approximation of the relation between E/P and E_p/P, which further depends on processes and parameters related to soil moisture dynamics, soil texture, land use and carbon exchange.

We use 17 global E (refs 18,27,28) and 6 observation-based global P data sets together with 21 estimates of E_p for the evaluation, resulting in a total of 2,142 combinations for the 1984–2005 period (see Methods and Supplementary Information for further information on all data sets). The data sets are interpolated onto a common $0.5° \times 0.5°$ global grid.

Each of the 2,142 possible combinations of the 1984–2005 annual averages of E/P in conjunction with E_p/P corresponds to a point cloud (Fig. 1). We validate each point cloud against the adjusted Budyko curve (equation (1)) using a modified root mean square error that penalizes data points overshooting the supply ($E/P > 1$) or demand limits ($E/E_p > 1$) by assigning higher weights (Methods). We refer to this measure as the root-mean-square-weighted error (RMSwE). A low RMSwE indicates a reasonable realism of a data set combination in terms of the Budyko approximation.

[1]Institute for Atmospheric and Climate Science, ETH Zurich, Universitaetsstrasse 16, 8092 Zurich, Switzerland, [2]Center for Climate Systems Modeling (C2SM), ETH Zurich, Universitaetsstrasse 16, 8092 Zurich, Switzerland, [3]Department of Civil and Environmental Engineering, Princeton University, Princeton, New Jersey 08544, USA, [4]Max Planck Institute for Biogeochemistry, 07745 Jena, Germany. †Present address: Climate Research Division, Environment Canada, Toronto, Ontario M3H 5T4, Canada. *e-mail: peter.greve@env.ethz.ch; sonia.seneviratne@ethz.ch

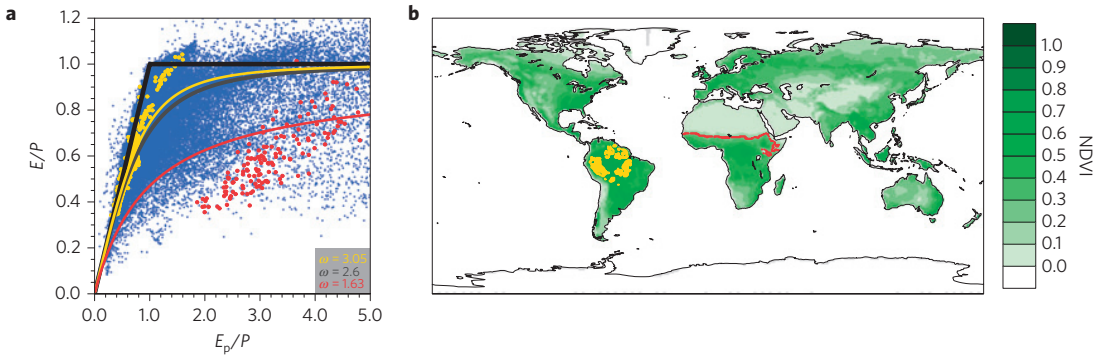

Figure 1 | Vegetation-adjusted Budyko framework. a, Point cloud of climatological E/P versus E_p/P from all grid points, taken from one combination of E, P and E_p data sets (NOAH E, CRU P and Princeton E_p data sets, see Supplementary Information) within the Budyko space. Black lines illustrate the demand ($E=E_p$) and supply limit ($E=P$). The Budyko curve (dark grey) in its original formulation ($\omega=2.6$) does not account for land surface properties. Equation 1 adjusted to climatological NDVI of about 0.8 over Amazonia (dark yellow) and about 0.2 over Africa (red) exhibits a better fit to the corresponding grid points. **b**, Climatological NDVI for the 1984–2004 period. Red and yellow colour denotes grid points with NDVI values of 0.2 over Africa and 0.8 over Amazonia, respectively as in **a**.

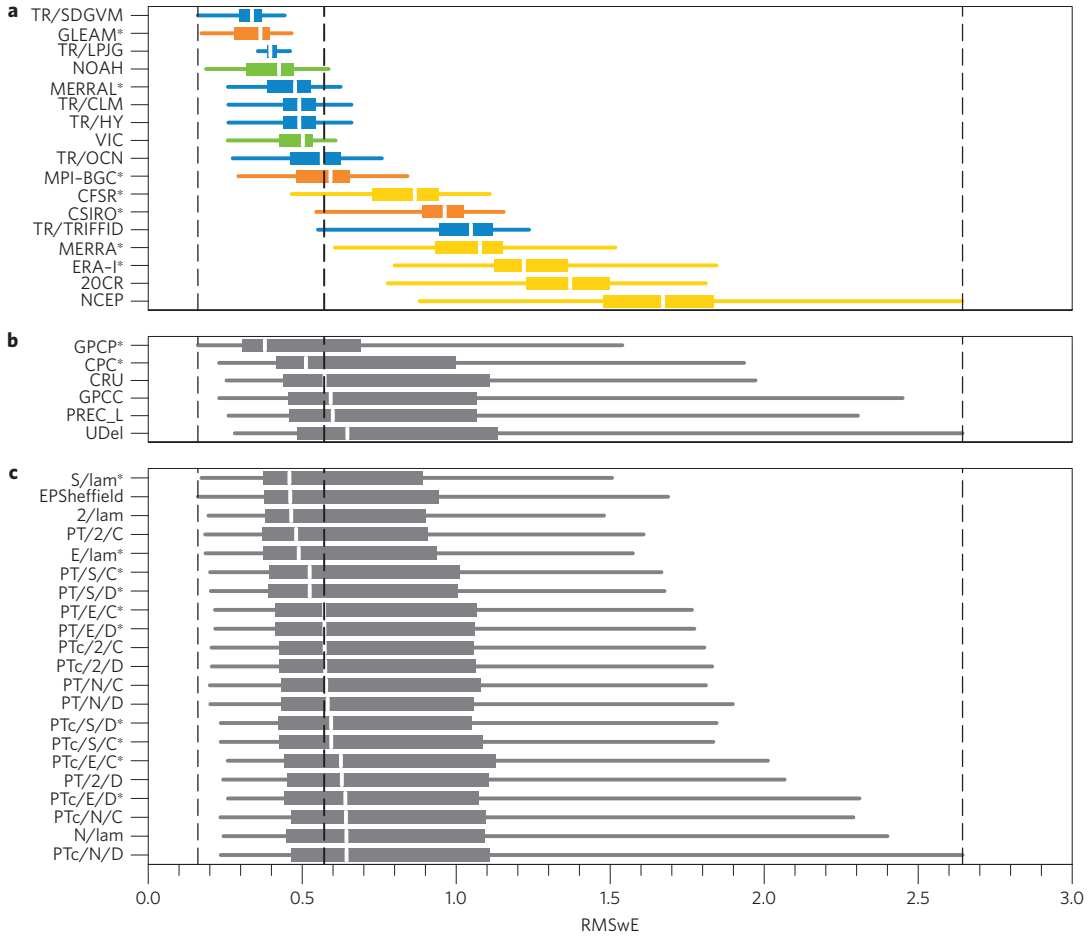

Figure 2 | Budyko validation of hydrological data set combinations for the 1984–2005 period. a–c, Box plots of all RMSwEs related either to an individual E (**a**), an individual P data set (**b**) or the E_p estimates (**c**). Data sets not spanning the 1948–2005 period are marked with an asterisk. Colours for the E data sets denote the different classes[18]: observation-based 'diagnostic' data sets (orange), LSMs with various forcings (green), LSMs from the TRENDY (TR) project[28] (blue), reanalysis (yellow). Dashed vertical lines illustrate the absolute minimum, the overall median and absolute maximum RMSwE (from left to right). See text and Supplementary Information.

The RMSwE values of all combinations of the considered E, P and E_p data sets are shown in Fig. 2. Clearly, the highest uncertainty lies in the choice of the E data sets, which are derived from various different sources and models. The E data sets at the top of the panel show lower error measures compared with those at the bottom of the panel, independently of the choice of P and E_p. Thus, the choice of the P and E_p data sets is almost arbitrary. However, the Global Precipitation Climatology Project (GPCP) data set slightly outperforms the other P data sets.

We use the 1984–2005 validation period to include a large number of both model- and observation-based data sets. To assess long-term dryness changes, only model-based data sets of E cover sufficiently long periods. For the analysis of dryness changes, we switch to the 1948–2005 period, which provides a good trade-off between a sufficient subset of data set combinations and a long enough time period to analyse changes. We use 7 E data sets with median RMSwE below the overall median (Fig. 2) spanning the longer period in combination with 4 P and 11 E_p data estimates. Note that the corresponding validation of these data sets for the longer period yields consistent results (Supplementary Information).

To analyse long-term hydrological changes we compare differences between the 1948–1968 and 1985–2005 periods, considering both changes in water availability (evaluated from the comparison of ΔP and ΔE) and changes in climate aridity/humidity (evaluated from the comparison of ΔP and ΔE_p). We compute climatologies to be consistent with previous studies[8,10] and the Budyko framework. Note that our results are not qualitatively affected by the exact definition of these time periods (Supplementary Information). On the basis of this approach, we identify drying trends in water availability in regions with $\Delta E > \Delta P$ (and respectively wetting trends in regions with $\Delta E < \Delta P$), and regime shifts towards more arid (humid) conditions in regions with $\Delta E_p > \Delta P$ ($\Delta E_p < \Delta P$). By doing so we give consideration to the different hydroclimatological characteristics of the land surface in comparison with the ocean, as the available water is limited there by both water storage and water supply. Thus, both changes in the water supply (P) and storage depletion/accumulation (changes in E and E_p) need to be jointly considered.

For each grid point, we obtain 28 (77) combinations for ΔE, ΔP (ΔE_p, ΔP), which we plot in the respective phase spaces (Fig. 3). The deviation of a point cloud from the line of no change (the identity function) is quantified by the Mahalanobis distance and significance is assigned using the F-distribution (Methods).

A striking feature is the large fraction (75.4%) of land area with non-significant changes, which is primarily a result of data uncertainty although interannual and decadal variability could also play a role[7].

Areas undergoing significant changes ($p < 0.05$) towards drier/wetter conditions regarding combinations of (ΔP, ΔE), (ΔP, ΔE_p) or both are shaded in Fig. 4a. Changes towards more arid conditions (red/orange) are found in many parts of Africa, especially in the Sahel and eastern Africa, eastern Asia, eastern Australia and partly in the western Mediterranean and northeastern Brazil. In contrast, drying trends in the northern Mediterranean and small parts of the Sahel are due to changes in the water availability (pink/green). Note that the identified changes in dryness in the Sahel region are unlikely to have been due to changes in greenhouse gas forcing, as there is a wettening in recent years[3] and analyses have suggested that changes in large-scale circulation patterns due to aerosol forcing may be relevant for these[29]. In addition, local changes in dryness are also strongly influenced by changes in large-scale circulation patterns (for example, decadal changes in El Niño/Southern Oscillation for tropical rainfall over land[13]). Significant drying trends in both the water availability and hydrological regime are sparse and primarily found in parts of western Africa. Wetting trends are located in eastern North America, parts of South America and Australia. These results confirm previous findings regarding long-term changes[3], such as for example, drying trends in the Mediterranean and eastern Asia, and wetting in eastern North America. They also highlight changes over eastern Africa (drying) and parts of South America (wetting).

To evaluate the DDWW paradigm in areas undergoing significant changes, every grid point is additionally classified as either arid ($E_p/P > 2$) or humid ($E_p/P < 2$) over the 1948–1968 period[20]. Regions not significantly classified as either arid or humid are denoted as transitional climate regimes[17]. The classification of each grid point uses the same Mahalanobis distance-based approach as for the drying trends (see Fig. 3 and Methods for more details). The resulting pattern (Fig. 4b) is in good agreement with the commonly used standard climate-classifications of Köppen–Geiger[30].

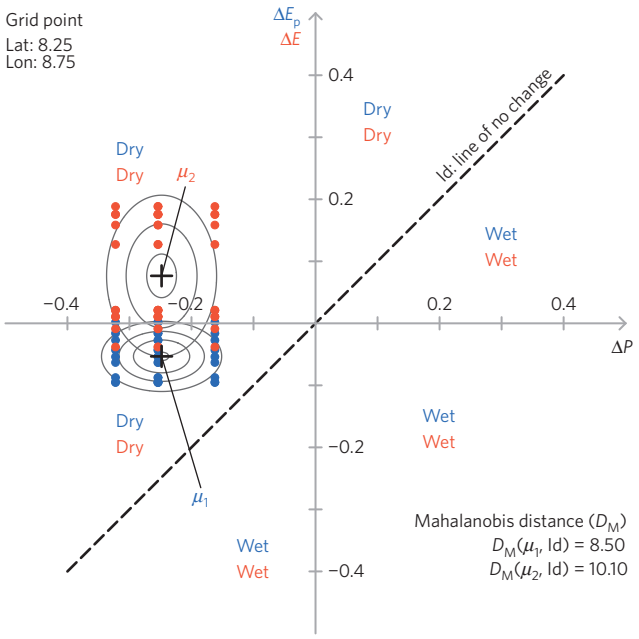

Figure 3 | Detection of robust dryness changes. Point clouds of ΔP against ΔE (red) and ΔE_p (blue) for a particular grid point (8.25° N, 8.75° E). To each point cloud with its corresponding centre of mass (μ) we fit a bivariate normal distribution. Values above the identity line (line of no change) correspond to drying hydroclimatological conditions. The Mahalanobis distance is measured to the identity line and significance is assigned following a Fisher distribution (Methods). This example shows a significant shift towards drier conditions regarding the land water balance and in terms of hydrological regime shift (note that $\Delta P_{CRU} = -0.2538$ and $\Delta P_{PREC/L} = -0.2541$ are very similar and thus almost not distinguishable). Units are millimetres per day.

A systematic comparison of both changes and climatological hydrological conditions of the early 1948–1968 period allows us to evaluate the DDWW paradigm (Fig. 4c) for historical changes. The paradigm is proved to be invalid in the major fraction of the area with change. This particularly applies to large areas classified as humid south of the Sahel, in Central and Eastern Africa, north of the Mediterranean and parts of East Asia, which all experienced significant drying. The area of wettening dry regions on the other hand is small. Note that significant changes are also found in transitional regions, generally towards drier conditions, such as for example, in eastern Asia, the western Mediterranean, small parts of eastern Australia and Africa. Altogether the area fraction where the DDWW paradigm is not valid (13.8%, including 4.3% transitional regions) is larger than the fraction in which it is confirmed (10.8%), highlighting that it does not apply to historical changes at annual timescales over land. However, changes at seasonal scales are not analysed in this study and may take place in some regions[9,14].

Our results emphasize that one should be careful when relying on simplifying statements such as the DDWW paradigm for assessments on historical dryness changes, which are potentially misleading as they do not fully account for the complexity of the underlying system. Note that several previous studies pointing to the DDWW paradigm include ocean areas in their analysis[8–11,13,14].

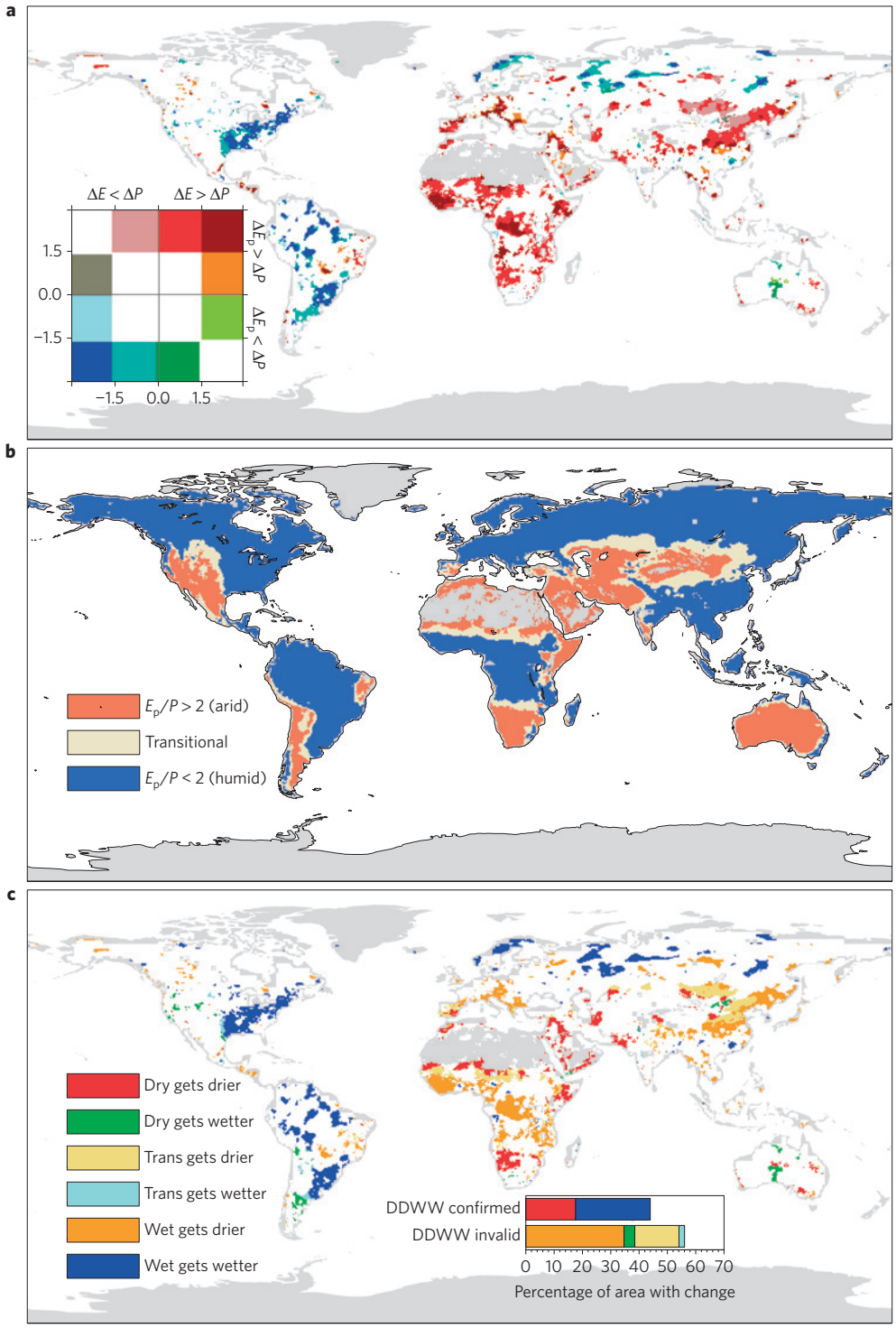

Figure 4 | Investigating the DDWW paradigm. a, Significant drying/wetting trends computed at the grid-box level. Dark red and dark blue denote a significant change towards drier and wetter conditions, respectively both regarding the land water balance and hydrological regime shifts. Red/orange shows a shift towards more arid conditions. Drying due to changes in the land water balance alone is depicted by green/pink. **b**, Distribution of arid (orange) and humid (blue) areas within the period from 1948 to 1968. Beige denotes transitional areas where no significant attribution is possible. **c**, Comparing the changes in **a** with the hydrological conditions in **b** yields an evaluation of the 'dry gets drier, wet gets wetter' paradigm. Red/dark blue colours indicate regions where the paradigm is found to be valid. Humid areas getting drier (orange) are widely found.

Whereas the DDWW paradigm possibly holds over the ocean (but using definitions of 'dry' and 'wet' regimes that are not applicable to land areas), our results clearly show that the DDWW is an oversimplification over land. In addition, previous findings[8,9,13] argue that patterns of P–E will be enhanced owing to increased moisture fluxes, implying solely a wet gets wetter response over land (although our analysis does also not confirm this feature for historical data). These issues were noted before[8,16], but are not addressed in the public discourse and so far no attempts have been made to account for the different hydroclimatological conditions

over land. Also note that previous studies assess seasonal[9,14] and/or large-scale/zonal changes[8–11,13,14], rather than mean annual changes at regional scales. Given the importance of regional dryness changes for socio-economic sectors, our results highlight that studies on changes in hydroclimatological conditions must not rely on single-variable data sets and dryness metrics to adequately assess the underlying uncertainties.

Methods

Evapotranspiration and precipitation data sets. The E data sets are subdivided into three categories[18,27]: 'diagnostic data sets', which are primarily derived from observations; land surface model (LSM)-based estimates driven by observation-based forcing; and reanalysis estimates. P data sets are either derived only from rain gauge observations, or from rain gauges in combination with satellite-derived estimates.

Potential evaporation estimates. We use here 3 common methods of differing complexity to determine E_p. Priestley–Taylor with a constant (PTc) or with a varying alpha parameter (PT) includes net radiation (R_n). The widely used method by Penman–Monteith (PM) additionally considers influences of vegetation and aerodynamic properties. E_p is also estimated directly from R_n (by dividing R_n with the latent heat of vaporization λ). By employing data sets of radiation and temperature, together with a pre-compiled 'dry' and 'wet' PM data set[6], 21 estimates of global E_p are used. Several studies have shown that temperature-based E_p estimates are not suitable for trends[6], and we thus do not use such estimates here. Nonetheless, we note that the results are not strongly affected if these are included (Supplementary Information). Further information on all data sets and methods is provided in the Supplementary Information.

Budyko evaluation. To account for vegetation influences, the Budyko curve (equation (1)) is adjusted using climatological NDVI (ref. 26), which relates linearly to the free parameter ω in equation (1).

$$\omega = 2.36 \cdot \left(\frac{\mathrm{NDVI} - \mathrm{NDVI}_{\min}}{\mathrm{NDVI}_{\max} - \mathrm{NDVI}_{\min}} \right) + 1.16$$

The RMSwE of a particular cloud of n points within the Budyko space is then calculated as

$$\mathrm{RMSwE} = \sqrt{\frac{\sum_{i=1}^{n} (w_i \cdot D_i)^2}{n}}$$

with w_i being the individual weight of point i. The ith deviation D_i is the Euclidean distance between point i and the adjusted Budyko curve, accounting for errors in both E/P and E_p/P at the same time. The weight w_i is calculated as

$$w_i = 1 + \sqrt{\frac{s_i}{1}}$$

with $s_i = 0$ for all points within the limits ($E/P \leq 1$ and $E \leq E_p$). Outside the limits we assign the Euclidean distance between point i and the limits to s_i. Thus, w_i is increasing relatively fast for small overshoots, but more slowly for large overshoots to reduce the influence of possible outliers. A perfect fit of a point cloud to the adjusted Budyko curve results in a zero RMSwE.

Mahalanobis distance and significance. To measure distance and its significance of a point cloud from the no-change line within the (ΔP, ΔE) and (ΔE_p, ΔP) spaces, respectively, we calculate the Mahalanobis distance D_M. D_M is based on the covariance matrix Σ that provides a joint measure of data uncertainty in both variables of the respective point cloud,

$$D_M(\mu, \mathrm{Id}) = \sqrt{(\mu - \mathrm{Id})^T \Sigma^{-1} (\mu - \mathrm{Id})}$$

where μ denotes the centre of mass and Id the identity function (line of no change). As Id and the point cloud of the data estimates are completely independent, the distance distribution approximately follows an F-distribution

$$\frac{npD_M^2}{n-p} \sim F(p, n-p)$$

where n denotes the number of data points and p the degrees of freedom ($p = 2$ in a two-dimensional case). Significance at the 5% level is thus assigned for $n = 28$ combinations of E and P data sets if $D_M^2 \gtrsim 1.5$ and for $n = 77$ combinations of E and E_p data sets also if $D_M^2 \gtrsim 1.5$.

Classification of hydrological conditions. Aridity (or humidity, respectively) is assigned at the grid-box level if the Mahalanobis distance between the cloud of (P, E_p) data points and the $2 \cdot \mathrm{Id}$ line ($E_p/P = 2$) is significant ($p < 0.05$) following the above-mentioned F-distribution, and the centre of mass lies above (below) the $2 \cdot$ Id line. Regions not significantly classified as either arid or humid hydroclimatological conditions are denoted as transitional. Of all (non-missing) global land area, about 59% is classified humid, whereas about 25% is arid and 16% is transitional. It is important to note that many hyperarid regions (such as, for example, the Sahara) have missing data.

Received 11 April 2014; accepted 12 August 2014;
published online 14 September 2014;
corrected after print 24 September 2014

References

1. Piao, S. *et al.* The impacts of climate change on water resources and agriculture in China. *Nature* **467,** 43–51 (2010).
2. Hoekstra, A. Y. & Mekonnen, M. M. The water footprint of humanity. *Proc. Natl Acad. Sci. USA* (2012).
3. Seneviratne, S. I. *et al. Managing the Risks of Extreme Events and Disasters to Advance Climate Change Adaptation* 109–230 (Cambridge Univ. Press, 2012).
4. Burke, E. J. & Brown, S. J. Evaluating uncertainties in the projection of future drought. *J. Hydrometeorol.* **9,** 292–299 (2008).
5. Dai, A. Drought under global warming: A review. *Wiley Interdiscip. Rev.: Clim. Change* **2,** 45–65 (2011).
6. Sheffield, J., Wood, E. F. & Roderick, M. L. Little change in global drought over the past 60 years. *Nature* **491,** 435–438 (2012).
7. Orlowsky, B. & Seneviratne, S. I. Elusive drought: Uncertainty in observed trends and short- and long-term CMIP5 projections. *Hydrol. Earth Syst. Sci.* **17,** 1765–1781 (2013).
8. Held, I. M. & Soden, B. J. Robust responses of the hydrological cycle to global warming. *J. Clim.* **19,** 5686–5699 (2006).
9. Chou, C., Neelin, J. D., Chen, C-A. & Tu, J-Y. Evaluating the Rich-Get-Richer mechanism in tropical precipitation change under global warming. *J. Clim.* **22,** 1982–2005 (2009).
10. Durack, P. J., Wijffels, S. E. & Matear, R. J. Ocean salinities reveal strong global water cycle intensification during 1950 to 2000. *Science* **336,** 455–458 (2012).
11. Allan, R. P., Soden, B. J., John, V. O., Ingram, W. & Good, P. Current changes in tropical precipitation. *Environ. Res. Lett.* **5,** 025205 (2010).
12. Seager, R. & Vecchi, G. A. Greenhouse warming and the 21st century hydroclimate of southwestern North America. *Proc. Natl Acad. Sci. USA* **107,** 21277–21282 (2010).
13. Liu, C. & Allan, R. P. Observed and simulated precipitation responses in wet and dry regions 1850–2100. *Environ. Res. Lett.* **8,** 034002 (2013).
14. Chou, C. *et al.* Increase in the range between wet and dry season precipitation. *Nature Geosci.* **6,** 263–267 (2013).
15. Roderick, M. L., Sun, F. & Farquhar, G. D. Water cycle varies over land and sea. *Science* **336,** 1230–1231 (2012).
16. Roderick, M. L., Sun, F., Lim, W. H. & Farquhar, G. D. A general framework for understanding the response of the water cycle to global warming over land and ocean. *Hydrol. Earth Syst. Sci.* **18,** 1575–1589 (2014).
17. Seneviratne, S. I. *et al.* Investigating soil moisture-climate interactions in a changing climate: A review. *Earth-Sci. Rev.* **99,** 125–161 (2010).
18. Mueller, B. *et al.* Evaluation of global observations-based evapotranspiration datasets and IPCC AR4 simulations. *Geophys. Res. Lett.* **38,** L06402 (2011).
19. Vicente-Serrano, S. M., Beguería, S. & López-Moreno, J. I. A multiscalar drought index sensitive to global warming: The standardized precipitation evapotranspiration index. *J. Clim.* **23,** 1696–1718 (2009).
20. Middleton, N. *et al. World Atlas of Desertification* 2nd edn (Arnold, Hodder Headline, PLC, 1997).
21. Budyko, M. I. *Climate and Life* (Academic, 1974).
22. Fu, B. On the calculation of the evaporation from land surface (in Chinese). *Sci. Atmos. Sin.* **1,** 23–31 (1981).
23. Zhang, L. *et al.* A rational function approach for estimating mean annual evapotranspiration. *Water Resour. Res.* **40,** W02502 (2004).
24. Donohue, R. J., Roderick, M. L. & McVicar, T. R. On the importance of including vegetation dynamics in Budyko's hydrological model. *Hydrol. Earth Syst. Sci.* **11,** 983–995 (2007).
25. Roderick, M. L. & Farquhar, G. D. A simple framework for relating variations in runoff to variations in climatic conditions and catchment properties. *Wat. Resour. Res.* **47,** W00G07 (2011).
26. Li, D., Pan, M., Cong, Z., Zhang, L. & Wood, E. Vegetation control on water and energy balance within the Budyko framework. *Wat. Resour. Res.* **49,** 969–976 (2013).
27. Mueller, B. *et al.* Benchmark products for land evapotranspiration: LandFlux-EVAL multi-dataset synthesis. *Hydrol. Earth Syst. Sci.* **10,** 769–805 (2013).

28. Sitch, S. *et al.* Trends and drivers of regional sources and sinks of carbon dioxide over the past two decades. *Biogeosci. Discuss.* **10,** 20113–20177 (2013).
29. Hwang, Y-T., Frierson, D. M. W. & Kang, S. M. Anthropogenic sulfate aerosol and the southward shift of tropical precipitation in the late 20th century. *Geophys. Res. Lett.* **40,** 2845–2850 (2013).
30. Peel, M. C., Finlayson, B. L. & McMahon, T. A. Updated world map of the Köppen–Geiger climate classification. *Hydrol. Earth Syst. Sci.* **11,** 1633–1644 (2007).

Acknowledgements

The Center for Climate Systems Modeling (C2SM) at ETH Zurich is acknowledged for providing technical support. This work was supported by ETH Research Grant CH2-01 11-1. We acknowledge participants of the TRENDY model intercomparison project for access to their simulation results. These include, C. Huntingford (TRIFFID), B. Poulter (LPJ), A. Ahlström, A. Arneth, B. Smith (LPJ-GUESS), M. Lomas (SDGVM), P. Levy (HyLand), S. Levis, G. Bonan (NCAR-CLM4), S. Zaehle (OCN), N. Viovy (Orchidee), and S. Sitch and P. Friedlingstein (project coordinators). We acknowledge D. Miralles (University of Bristol) for access to the GLEAM data set. CRU data were obtained from the University of East Anglia Climate Research Unit (CRU), British Atmospheric Data Centre, 2008, available from http://badc.nerc.ac.uk/data/cru. The GPCP combined precipitation data were developed and computed by the NASA/Goddard Space Flight Centers Laboratory for Atmospheres as a contribution to the GEWEX Global Precipitation Climatology Project. GPCC precipitation data are available from the GPCC homepage: http://gpcc.dwd.de. CPC merged analysis of precipitation data, PREC/L precipitation data, NCEP reanalysis data, UDel air temperature and precipitation data were provided by the NOAA/OAR/ESRL PSD, from their website at http://www.esrl.noaa.gov/psd/. We acknowledge the Global Modeling and Assimilation Office and the GES DISC for the dissemination of MERRA and MERRA-LAND, and the ECMWF for the dissemination of ERA-Interim data. The CFSR data are from the Research Data Archive, which is maintained by the Computational and Information Systems Laboratory at the National Center for Atmospheric Research (NCAR). NCAR is sponsored by the National Science Foundation. The original data are available from the Research Data Archive at the National Center for Atmospheric Research, Computational and Information Systems Laboratory. http://rda.ucar.edu/datasets/ds093.2/. Support for the Twentieth Century Reanalysis Project data set is provided by the US Department of Energy, Office of Science Innovative and Novel Computational Impact on Theory and Experiment (DOE INCITE) program, and Office of Biological and Environmental Research (BER), and by the National Oceanic and Atmospheric Administration Climate Program Office. SRB data were obtained from the NASA Langley Research Center Atmospheric Sciences Data Center NASA/GEWEX SRB Project.

Author contributions

P.G., B.O. and S.I.S. designed the study and wrote the manuscript. P.G. performed all computations. B.M. provided support with the collection of evapotranspiration data sets. J.S. and M.R. provided data sets to the study. All authors commented on the manuscript.

Additional information

Supplementary information is available in the online version of the paper. Reprints and permissions information is available online at www.nature.com/reprints. Correspondence and requests for materials should be addressed to P.G. or S.I.S.

Competing financial interests

The authors declare no competing financial interests.

CORRIGENDUM

Global assessment of trends in wetting and drying over land

Peter Greve, Boris Orlowsky, Brigitte Mueller, Justin Sheffield, Markus Reichstein and Sonia I. Seneviratne

Nature Geoscience http://dx.doi.org/10.1038/ngeo2247 (2014); published online 14 September 2014; corrected after print 24 September 2014.

In the version of this Letter originally published, in the main text, the number of different combinations given for each grid point in Fig. 3 were incorrect and should have read '28 (77)'. Additionally, the second sentence describing the parameters in the final equation should have read "Significance at the 5% level is thus assigned for $n = 28$ combinations of E and P data sets if $D_M^2 \geq 1.5$ and for $n = 77$ combinations of E and E_p data sets also if $D_M^2 \geq 1.5$". Furthermore, in the key for Fig. 4a, the values should have read 1.5 (-1.5). These errors have no influence on the results of the study, and have now been corrected in the online versions of the Letter.